

Crystallization-Induced Properties from Morphology-Controlled Organic Crystals

Chibeom Park, Ji Eun Park, and Hee Cheul Choi*

Department of Chemistry, Pohang University of Science and Technology (POSTECH) and Center for Artificial Low Dimensional Electronic Systems (CALDES), Institute for Basic Science (IBS), San 31, Hyoja-dong, Nam-Gu, Pohang 790-784, Korea

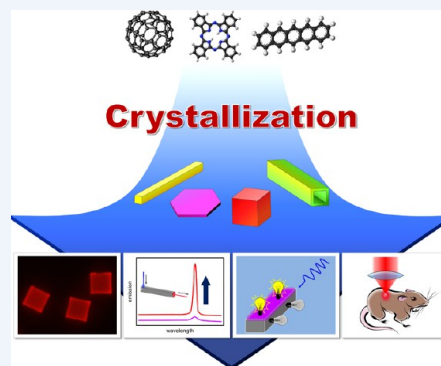
CONSPECTUS: During the past two decades, many materials chemists have focused on the development of organic molecules that can serve as the basis of cost-effective and flexible electronic, optical, and energy conversion devices. Among the potential candidate molecules, metal-free or metal-containing conjugated organic molecules offer high-order electronic conjugation levels that can directly support fast charge carrier transport, rapid optoelectronic responses, and reliable exciton manipulation.

Early studies of these molecules focused on the design and synthesis of organic unit molecules that exhibit active electrical and optical properties when produced in the form of thin film devices. Since then, researchers have worked to enhance the properties upon crystallization of the unit molecules as single crystals provide higher carrier mobilities and exciton recombination yields. Most recently, researchers have conducted in-depth studies to understand how crystallization induces property changes, especially those that depend on specific crystal surfaces.

The different properties that depend on the crystal facets have been of particular interest. Most unit molecules have anisotropic structures, and therefore produce crystals with several unique crystal facets with dissimilar molecular arrangements. These structural differences would also lead to diverse electrical conductance, optical absorption/emission, and even chemical interaction properties depending on the crystal facet investigated.

To study the effects of crystallization and crystal facet-dependent property changes, researchers must grow or synthesize crystals of highly conjugated molecules that have both a variety of morphologies and high crystallinity. Morphologically well-defined organic crystals, that form structures such as wires, rods, disks, and cubes, provide objects that researchers can use to evaluate these material properties. Such structures typically occur as single crystals with well-developed facets with dissimilar molecular arrangements. Recently, researchers have proposed several approaches for the vapor and solution phase synthesis of high quality organic crystals with various morphologies.

In this Account, we focus on methodologies for the synthesis of various organic- and metal-containing highly conjugated molecular crystals. We also examine the new optical and chemical properties of these materials. In addition, we introduce recent experimental results demonstrating that high crystallinity and specific molecular arrangements lead to crystallization-induced property changes. We believe that the understanding of the crystallization-induced property changes in organic crystals will provide both fundamental knowledge of the chemical processes occurring at various interfaces and opportunities for researchers to take advantage of crystallization-induced property changes in the development of high-performance organic devices.



1. INTRODUCTION

The size-dependent optical, electrical and chemical property changes of semiconducting and metallic materials, known as quantum size effect (QSE), have contributed to the birth and rapid advancement of nanoscience and nanotechnology. Among diverse interdisciplinary research subjects that have contributed to support and establish QSE, the “synthesis” of various materials exhibiting QSE has been one of the core subjects especially in chemistry fields. While a tremendous amount of effort has successfully granted a wide range of functional nanomaterials, most of the cases exhibiting QSE have been limited to inorganic materials as their quantized energy states are clearly represented by various physical properties, such as electrical transport, optical absorption, emission, and so forth upon the reduction of their sizes. Together with the fundamental studies of QSE from such

inorganic nanomaterials, another important research stream is to construct functional structures from molecules or preformed nanomaterials into higher dimensional structures through bottom-up approaches, such as self-assembly or self-organization. In this perspective, the expansion of the research target to *organic molecules*, especially highly conjugated molecules and their self-assemblies to multidimensional structures with characteristic functionalities, would further widen the candidate building blocks for future applications.

Contrary to the inorganic nanomaterials, organic molecule-based materials generally do not exhibit the size-dependent property changes when they shrink down from the bulks. The size-dependent property changes in organic crystals rather

Received: February 27, 2014

Published: June 5, 2014

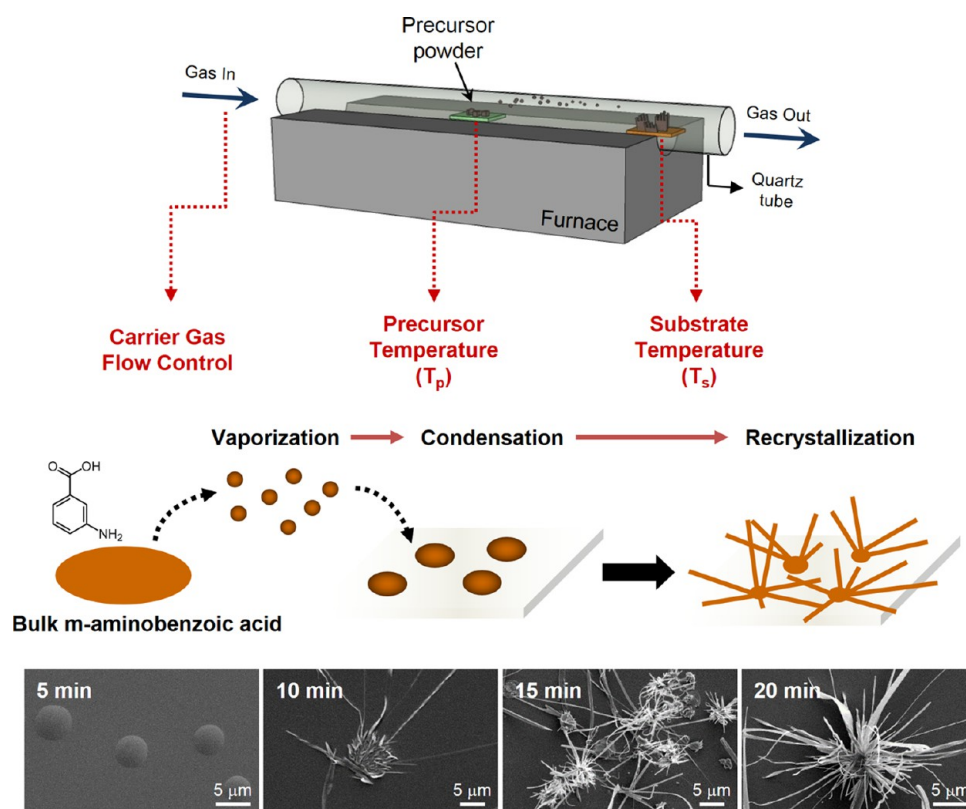


Figure 1. Schematic view of *f*-PVT setup and the mechanism of *m*-ABA helical nanobelt formation during *f*-PVT process. Reproduced with permission from ref 23 (Copyright 2010 WILEY VCH) and ref 24 (Copyright 2007 American Chemical Society).

frequently appear upon the gradual size increase through crystallization of organic molecules. Such an effect is called meso-size effect (MSE) and also called crystallization-induced effect (CIE) or aggregation-induced effect (AIE). The MSE indicates the new optical, electrical, chemical, and mechanical properties commencing from organic crystals while these properties are mostly silent when the corresponding molecules are present in an ensemble powder or solution form. The MSE further grants an opportunity to study many veiled phenomena, such as crystal facet-dependent property changes of organic crystals. The MSE is therefore a driving force for the development of new organic materials exhibiting various property changes upon the alteration of their crystal shapes. In this context, organic crystals formed into specific morphologies thus having well-developed crystal facets are ideal systems to study the morphology–property correlation.

To achieve this goal, the first mission is to synthesize organic crystals in various shapes. Nano- or micrometer scale organic crystals in wires, belts, tubes, rods, disks, and cubes composed of highly conjugated organic molecules such as fullerene,^{1–6} phthalocyanine,^{7–10} polyacene,^{11–14} and so forth having high quality and diverse crystal facets have been recently synthesized and examined for the crystallization-induced property change. In this Account, recent progress on the synthesis of geometrically well-defined highly conjugated molecule-based crystals and new optical, optoelectrical and chemical properties commencing from these crystals will be discussed. The investigation on the molecular arrangement-dependent property changes in organic crystals will provide fundamental knowledge about the behavior of electrons, photons and their mutual interactions at the molecular level, which will suggest a

new strategy for achieving high-performance organic molecule-based devices.

2. SYNTHESIS OF MORPHOLOGY-CONTROLLED ORGANIC CRYSTALS

Since most of the highly conjugated unit molecules have anisotropic structures, the molecular arrangements on each crystal facet would vary distinctly when the unit molecules are crystallized into specific morphologies. The optical, electrical, and chemical properties emerging from each crystal facet therefore would be largely different. For example, the absorption and emission processes are known to be primarily dependent on the relative orientation of induced dipole moment present in unit molecules and the electric component of incident lights.^{15,16} So, the constituent organic molecular units having specific arrangements on each crystal facet will govern the entire optical and chemical properties of the organic crystals. To evaluate such an effect on optical and chemical properties, it is most critical to develop synthetic methods yielding highly conjugated molecular crystals in various morphologies with well-developed crystal facets.

2.1. Physical Vapor Transport (PVT) Method

The physical vapor transport (PVT) process has been widely employed to prepare various organic and inorganic crystals. The PVT is generally performed at elevated temperature in a vacuum-sealed tube filled with precursors in either vertical or horizontal direction. The vacuum PVT process is advantageous over conventional solid-state reactions as (1) it accommodates various types of source, for example, chunks, powder, wire, and chips, and (2) it produces high purity thin films¹⁷ or crystals¹⁸ over large area owing to the vacuum condition that prohibits

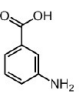
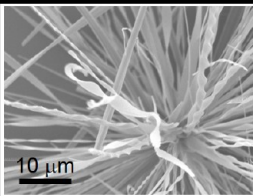

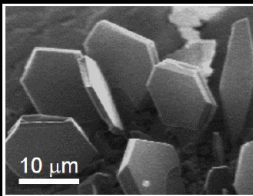
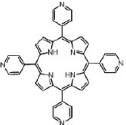
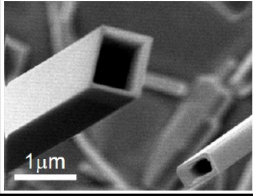
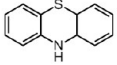
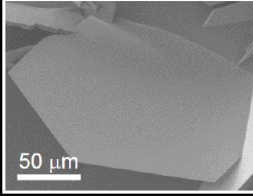
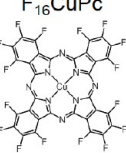
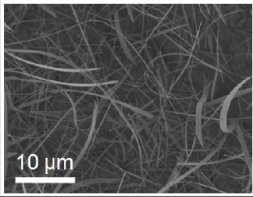
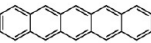
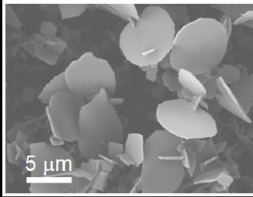
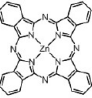
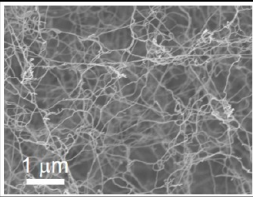
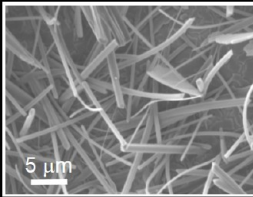
Unit Molecule	Crystal Geometry	Experimental Conditions	Unit Molecule	Crystal Geometry	Experimental Conditions
m-ABA 		170 °C 80 °C 100 sccm 40 min	C ₆₀ 		650 °C 500 °C 100 sccm 30 min
H ₂ TPyP 		450 °C 350 °C 100 sccm 30 min	Phenothiazine (PTZ) 		180 °C 40 °C 800 sccm 30 min
F ₁₆ CuPc 		500 °C 360 °C 100 sccm 40 min	Pentacene 		325 °C 180 °C 60 sccm 15 min
ZnPc 		550 °C 180 °C 800 sccm 50 min		350 °C 210 °C 100 sccm 15 min	

Figure 2. Various morphologies of conjugated molecular crystals obtained by *f*-PVT process and their growth conditions. The experimental conditions are listed in order of precursor temperature (red), substrate temperature (blue), carrier gas flow rate, and reaction time. Reproduced with permission from ref 3 (Copyright 2008 WILEY VCH), ref 7 (Copyright 2010 The Royal Society of Chemistry), ref 8 (Copyright 2012 Nature Publishing Group), ref 11 (Copyright 2012 WILEY VCH), ref 24 (Copyright 2007 American Chemical Society), ref 25 (Copyright 2009 WILEY VCH), and ref 26 (Copyright 2013 American Chemical Society).

side reactions such as oxidation and hydration. Considering that the conventional PVT is governed by thermodynamic equilibrium at designated reaction temperature, however, a greater chance to obtain crystals in diverse morphologies is available when the PVT process is operated out of vacuum, instead of under the continuous flow of inert gas, such as Ar, He, and N₂, as such a system allows kinetic controls.¹⁹ For example, the flow-type PVT (*f*-PVT) process consents the nucleation of precursor molecules followed by growth of crystals under the control of reaction parameters, such as kind, flow rate and pressure of carrier gas to induce the gradient of precursor vapor concentration as well as the gradient of temperature between the precursors and product collecting substrates.^{20–22}

The *f*-PVT process follows three specific growth steps: vaporization, condensation, and recrystallization steps, hence also called as VCR process as illustrated in Figure 1.²⁴ During the vaporization step, the precursor powder (e.g., *m*-amino-benzoic acid) is vaporized from the center region and transported by the carrier gas to the end region where the sample-collecting substrate is placed. The second step is condensation of the transported vapors onto the substrate, which is driven by naturally lowered temperature at the sample-collecting region. Note that further accurate tuning of precursor and substrate temperature can be achieved by using a two-zone heating furnace. Once condensates are populated, extra

transported vapors are likely to be saturated in the condensates and recrystallized into specific shapes. The precursor candidates are spanning from molecules based on single benzene ring to highly conjugated metal-free or metal containing molecules. Tetra(4-pyridyl)porphyrin (TPyP) rectangular nanotube (RNT),²⁵ hexadecafluorophthalocyanine (F₁₆CuPc) ribbon,⁷ zinc phthalocyanine (ZnPc) nanowire,⁸ C₆₀ hexagonal disk,³ phenothiazine (PTZ) disk,²⁶ and pentacene wire/disk structures¹¹ synthesized from respective molecules by *f*-PVT process are listed in Figure 2.

One of the most important advantages of *f*-PVT over conventional solid and solution phase crystallization methods is that the *f*-PVT yields series of kinetic products having various morphologies by altering carrier gas flow rate, precursor temperature (*T_p*), and sample collection temperature (*T_s*). Thus, the *f*-PVT can be considered as a kind of combinatorial method that has been applied for the drug discovery.²⁷ The crystal morphology is mainly determined by the preferred intermolecular interactions that are unique for each unit molecules and that develop crystal planes growing into major and minor crystal facets in order of surface energy at a given growth condition. The *f*-PVT frequently allows the preferential growth along the thermodynamically less favorable crystal planes by the small changes of reaction temperature. For example, both pentacene 1D wires and 2D disks are selectively synthesized by *f*-PVT process at 350 and 325 °C of *T_p*,

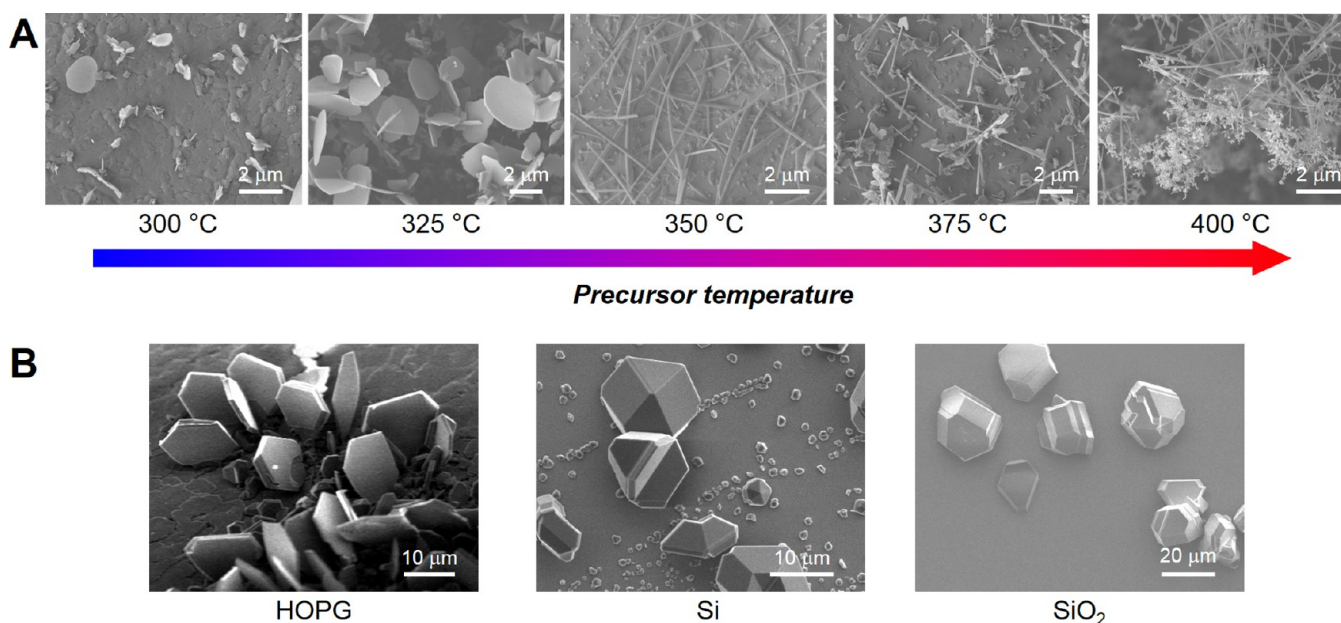


Figure 3. SEM images representing (A) influence of precursor temperature on the morphology of pentacene crystals. Reproduced with permission from ref 11. Copyright 2012 WILEY VCH. (B) Substrate dependence in C₆₀ disk growth. Reproduced with permission from ref 3. Copyright 2008 WILEY VCH.

respectively (Figure 3A), despite the fact that pure pentacene is known to preferentially grow into 2D disks only by conventional growth methods. The formation of pentacene 1D wire is the result of outgrowth from the sidewall of pentacene 2D disk, that is, {110} planes, resulting in the presence of a (010) plane in the wire that has the highest surface energy (6.4 meV/Å²) among the available planes of pentacene crystal.²⁸

Another factor affecting the shape of the crystal is the type of substrate. Basically any substrate including Si and SiO₂ is eligible for the reaction as long as the substrate is resistant to high thermal energy. Because the lattice parameters of organic crystals are usually much larger than that of crystalline substrate, epitaxial growth is not a general process for *f*-PVT. Nonetheless, the substrate surface occasionally influences the condensation step of crystal growth, and eventually the final morphologies of the crystals when the precursor molecule and substrate have electronic structural resemblance. For example, hexagonal C₆₀ disk crystals are dominantly obtained on a highly oriented pyrolytic graphite (HOPG) substrate, while three-dimensional irregular shape crystals are formed on Si or SiO₂ wafers (Figure 3B).

2.2. Solution Phase Crystallization Method

Together with *f*-PVT process, solution phase process has been also intensively studied for the crystallization of highly conjugated molecules in various morphologies. Based on the strategy rooted from the traditional solution phase recrystallization process, several modified methods including drop-drying, solvent vapor annealing (SVA), and liquid–liquid interface precipitation (LLIP) have been recently developed. One distinctive difference of solution phase crystallization from vapor phase one is the presence of solvent, which mediates the crystallization to start upon the local concentration change of solute at the liquid–air–solid, vapor–solid, and liquid–liquid interfaces. In addition to the role as a crystallization medium, solvent molecules can participate in the crystallization process more directly by intercalating themselves into the lattice of

target organic crystals through the occupation of void spaces (e.g., interstitial sites).

The solution phase crystallization of fullerene molecules exemplifies such a case. The pristine C₆₀ crystal having a face-centered cubic (fcc) structure allows relatively large interstitial sites²⁹ that can be occupied with versatile chemical species such as alkali metal atoms,^{30,31} halogen molecules,³² and small hydrocarbon molecules,³³ as well as solvent molecules (Figure 4A). The intercalation of solvent molecules into the lattice of fullerene induces the alteration of molecular arrangement to minimize overall lattice energy and provides an opportunity to grow the crystal into anisotropic morphology due to lowered symmetry. Indeed, fullerene crystals having various shapes like rectangular nanorod,³⁴ nanowire,³⁵ hexagonal nanosheets,³⁶ and microribbons³⁷ are obtainable by the solution processes, while only one meaningful shape (disk) is achieved by vapor phase reaction.³ Solvent molecule intercalation during crystallization is an efficient approach to control the crystal shape, which serves a good model system to evaluate the morphology-dependent property changes.

The effect of solvent has been elucidated by the demonstration of solvent-specific morphology control of C₆₀ crystals prepared by drop-drying process⁴ which provides simpler crystallization environment by avoiding the effect of secondary solvent required in LLIP method (Figure 4B). When *pseudo* 1D (*n*-hexane), 2D (mesitylene, *m*-dichlorobenzene, *m*-xylene), and 3D solvents (CCl₄ and SnCl₄) are used, C₆₀ molecules are grown into 0D dots, 1D wires, and 2D hexagonal disks, respectively. Especially, C₆₀ 1D wires are realized only with benzene-series *pseudo* 2D solvents having substituted functional groups at 120° apart each other (i.e., at *meta* positions), irrespective of polarity, type, and number of functional groups. According to the X-ray and electron diffraction results, all of C₆₀ wires and hexagonal disks have the crystal structures identical to those of *m*-xylene- and CCl₄-containing bulk C₆₀ crystals,^{38,39} respectively, suggesting that the solvent molecules are included in the lattice. These results

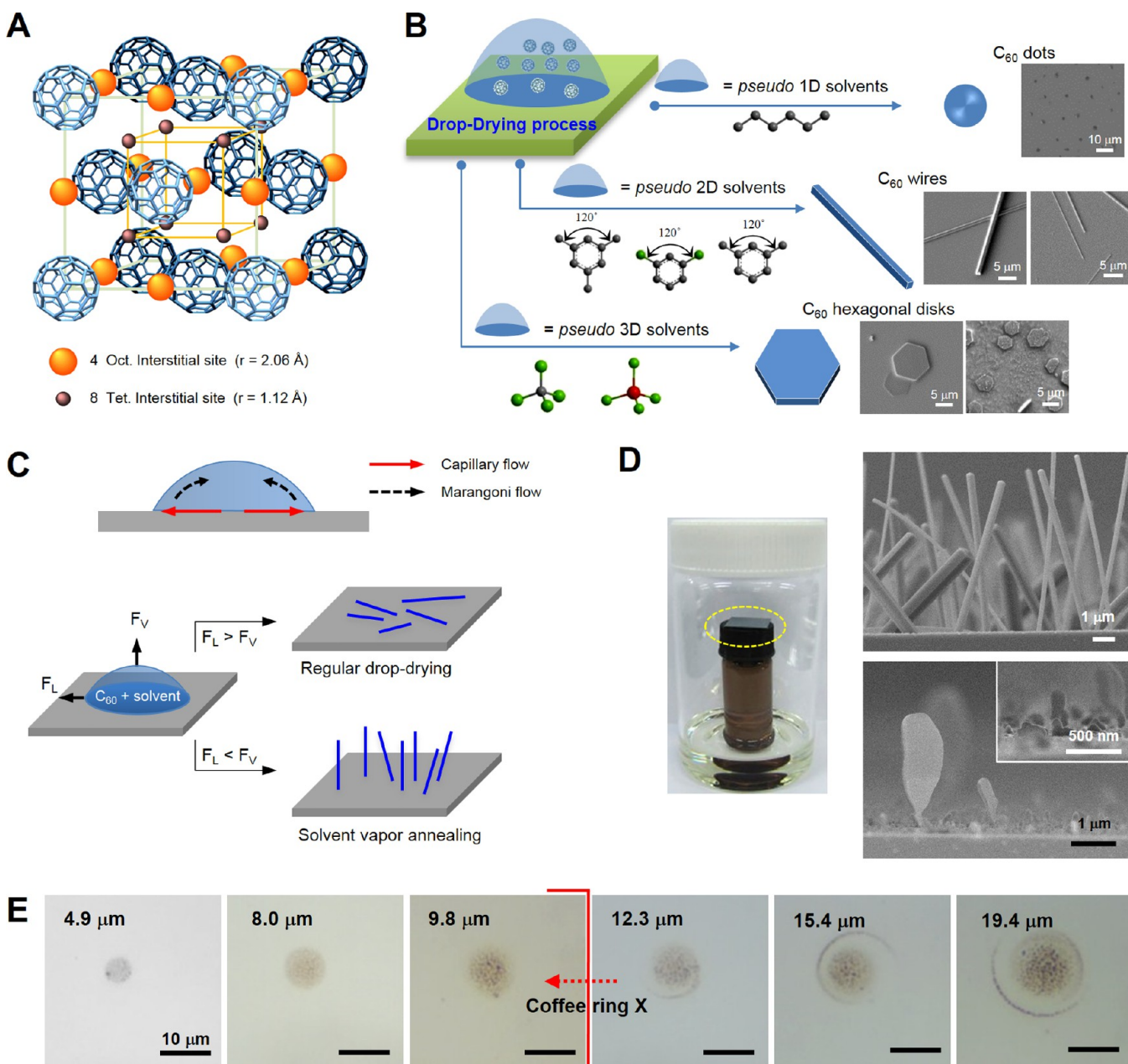


Figure 4. (A) Face-centered cubic structure of pristine C_{60} molecular crystal and available interstitial sites. (B) Morphology of C_{60} crystal determined by the molecular shape of solvent used in drop-drying process. Reproduced with permission from ref 4. Copyright 2009 The Royal Society of Chemistry. (C) Schematic representation of drop-drying and SVA process. (D) Apparatus for SVA process and vertically grown C_{60} wires (top) and disks (bottom). (E) Coffee ring formation depending on the size of single droplet of C_{60} solution in *m*-xylene. Reproduced with permission from ref 5. Copyright 2013 American Chemical Society.

imply that solvent molecules are cocrystallized with C_{60} , and the molecular shape of solvent is the primary determinant on the final morphology of C_{60} crystal.

The drop-drying process is facile but lacks of controllability in growth direction as most of the products are randomly oriented and deposited on a substrate laterally. The direction of crystal growth is mainly ruled by the drying force applied to a droplet at the boundaries formed by solution droplet and substrate. In the case of regular drop-drying process, there is a pinning of solution droplet on a substrate, and the evaporation of the solution induces outward capillary flow to replenish dried solvent.⁴⁰ This flow competes to circulating flow (Marangoni flow) induced by thermal or concentration gradient. Overall,

the competition of capillary and Marangoni flow exerts versatile forces on the crystallization process, where lateral force of solvent (F_L) becomes dominant over vertical force (F_V) in the regular drop-drying process (Figure 4C).

It has been found that F_V becomes dominant with minimization of F_L as the droplet size is smaller than about 10 μm , which is indirectly confirmed by the absence of accumulated crystals, called “coffee ring” (Figure 4E). However, the insufficient amount of C_{60} molecules in such small droplets does not result in any meaningful shape of crystals. Therefore, another crystallization methodology satisfying both the minimization of solution droplet size and sufficient supply of C_{60} molecules has been developed by adopting solvent vapor

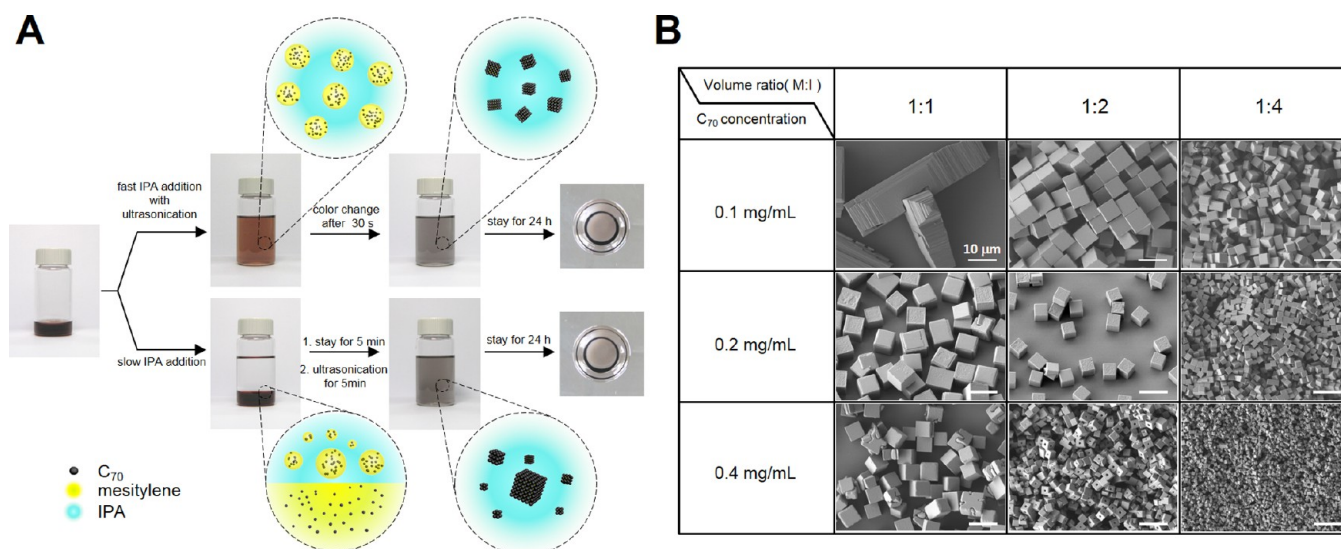


Figure 5. (A) Experimental procedures and crystallization mechanism in modified (top) and regular (bottom) LLIP method. (B) C₇₀ cube crystals obtained by LLIP at various concentration conditions. Reproduced with permission from ref 6. Copyright 2010 WILEY VCH.

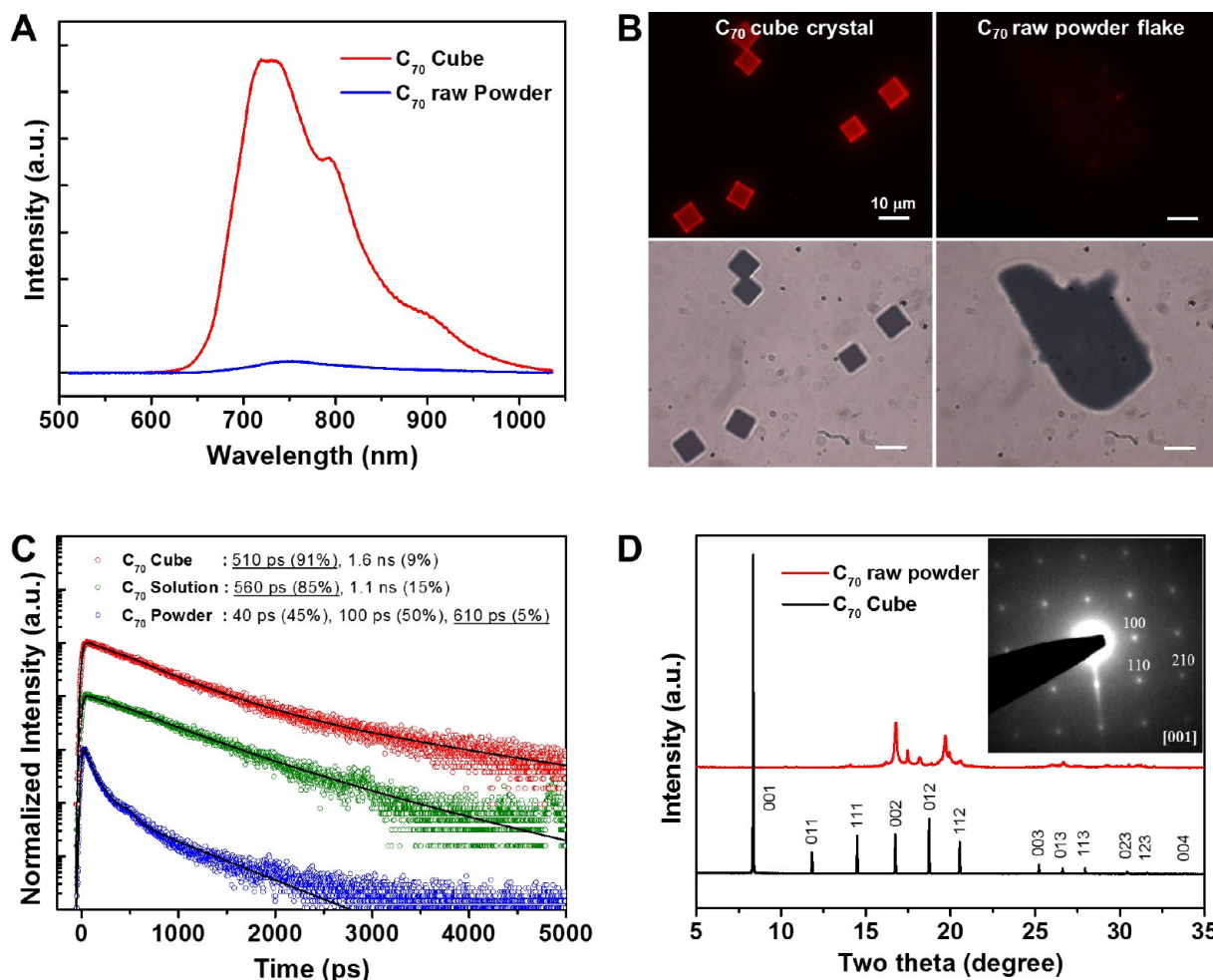


Figure 6. (A) PL spectra of C₇₀ cube crystals and C₇₀ powder. (B) Fluorescence microscope images (top row) and corresponding transmission optical microscope images (bottom row) of C₇₀ cube crystals and C₇₀ powder flake. (C) Time-resolved PL spectra measured at 750 nm and decay time constants. The main radiative decay component is underlined for each case. (D) XRD and SAED (inset) of C₇₀ cubes. All figures except the XRD data (red) in panel (D) are reproduced with permission from ref 6. Copyright 2010 WILEY VCH.

annealing (SVA) process. For this, precursor molecules (e.g., C₆₀) are predeposited on a substrate, which is then exposed to

solvent vapor that are under dynamic equilibrium in a closed reactor (left image in Figure 4D). The SVA environment allows

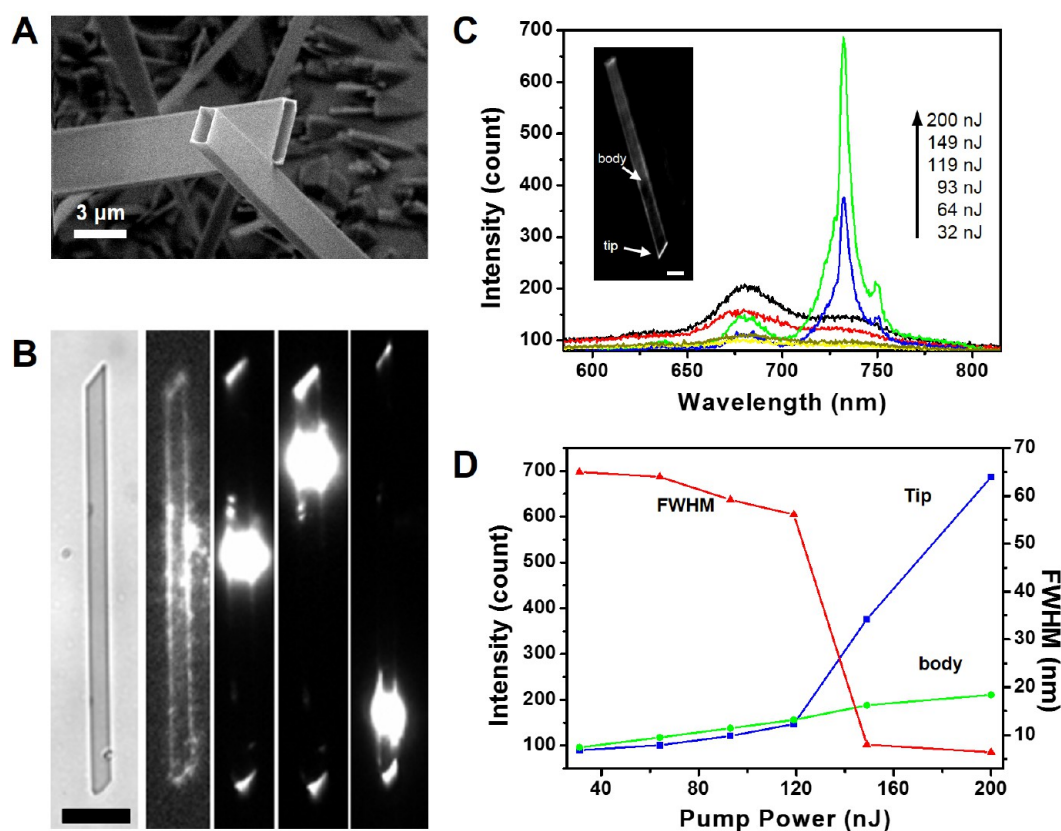


Figure 7. (A) SEM image of H_2TPyP RMTs. (B) Waveguiding phenomena observed in PL images of single H_2TPyP -RMT. The first and second images are bright field and epi-PL image, respectively, and the other three images are PL images obtained with focused spot illumination (Scale bar: $5 \mu\text{m}$). (C) PL spectra collected from the tip of a single H_2TPyP RMT depending on the excitation pump power. (D) Intensity and fwhm of 0–1 band emission as a function of excitation pump power. Reproduced with permission from ref 42. Copyright 2011 American Chemical Society.

continuous wetting and evaporation of droplets with dominant F_V . As a result, vertical C_{60} 1D wires and 2D disks are obtained from thermally evaporated C_{60} film under the dynamic equilibrium environment with *m*-xylene and CCl_4 vapors, respectively⁵ (right images in Figure 4D). In these cases, the correlation between the molecular shape of solvent and the final morphology of C_{60} crystal still retains well as in the case of regular drop-drying process.

The LLIP method, developed by Miyazawa et al.,⁴¹ also grants fullerene crystals in various morphologies, especially the fullerene crystals that are difficult to be obtained by the methods discussed earlier. For example, C_{70} cubes are obtained only by the LLIP method by direct precipitation at the interfaces of mesitylene (good solvent) and isopropyl alcohol (IPA, poor solvent).⁶ As shown in the bottom row of Figure 5A, slow addition of poor solvent forms an interface separating IPA and C_{70} containing mesitylene layers, where nucleation starts as diffusive mixing of two liquids occurs. Complete mixing of two liquids with a help of ultrasonication abruptly decreases overall solubility of the solution, resulting in the formation of C_{70} cube crystals. The homogeneity of C_{70} cube crystal can be further enhanced by fast injection of IPA with simultaneous application of ultrasonication, and the homogeneous liquid–liquid interface formation dramatically narrows the size distribution of C_{70} cubes (top row of Figure 5A and images in Figure 5B).⁶ Moreover, the average size of C_{70} cube is readily controlled by (1) changing the volume ratio of C_{70} solution in mesitylene to IPA and (2) changing C_{70} concentration in mesitylene, which modulate the size of the

microcavity and the number of nucleation sites, respectively (Figure 5B).

3. CRYSTALLIZATION-INDUCED PROPERTIES OF ORGANIC CRYSTALS

One of the foremost scientific findings that is drawn from organic crystals in various morphologies is to discover unprecedented crystallization-induced properties or morphology-dependent property changes. Examples below describe abnormal change of optical and chemical properties emerged from organic crystals, such as enhanced photoluminescence (PL) and optical waveguiding effects from fullerene, porphyrin, and pentacene crystals, as well as unprecedented water dispersibility from zinc phthalocyanine (ZnPc) nanowires.

3.1. Photoluminescence Enhancement in C_{70} Cubes

The PL from noncrystalline aggregates of highly conjugated molecules is generally suppressed because the irregular interparticle interactions in random aggregates induce new density of states between the frontier orbitals that play as nonradiative exciton decay pathways. The enhancement of PL of highly conjugated molecules thus can be fulfilled by achieving high level ordering of molecules upon crystallization as demonstrated from C_{70} cubes synthesized by LLIP method. The PL spectra and fluorescent microscope images from C_{70} cubes and powder show drastic difference in their intensities. The PL intensity from C_{70} cube at room temperature is approximately 30 times higher than that from C_{70} powder (Figure 6A). The possibility of enhancement by the presence of solvent molecules in C_{70} cube crystal is excluded as the solvent-

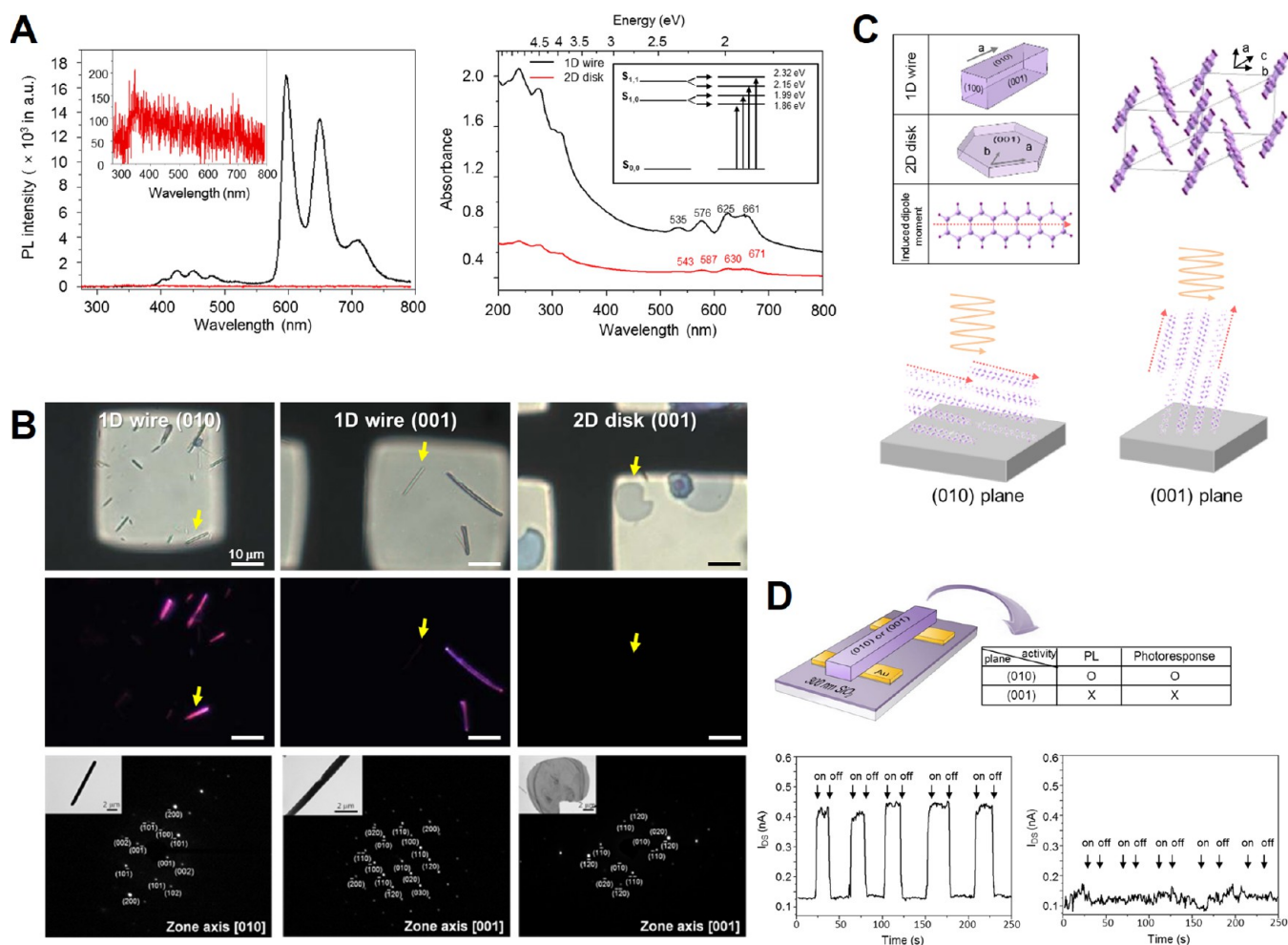


Figure 8. (A) PL (left) and absorption (right) spectra of pentacene 1D wire (black) 2D disk (red). Insets of the left and right graphs show an enlarged PL spectrum of pentacene 2D disk and a energy-level diagram for excitonic states of pentacene molecules, respectively. (B) Optical microscope (top row), PL (middle row), and electron diffraction pattern (bottom row) images of pentacene 1D wires and 2D disk depending on crystal planes. (C) Mechanism for the crystal surface-dependent PL activity. (D) Crystal surface-dependent electric photoresponse of pentacene 1D wire. Reproduced with permission from ref 11. Copyright 2012 WILEY VCH.

free C_{70} crystal obtained after thermal annealing still shows much higher PL intensity than C_{70} powder. Such a contrastive PL is also observed by fluorescence microscope images as the PL image of C_{70} cubes shows bright red emission color whereas negligible visible color is observed from C_{70} powder flakes (Figure 6B).

The time-resolved PL (TRPL) results obtained at the emission wavelength of 750 nm show that the portion of radiative decay component in C_{70} powder (5%) increases to about 90% in C_{70} cubes, which is comparable to homogeneous C_{70} solution (85%) (Figure 6C). The increased portion of radiative decay component in C_{70} cube is attributed to the long-range ordering of C_{70} molecules, by which the nonradiative decay path is efficiently minimized. The high-level ordering of C_{70} molecules is confirmed by the intense X-ray diffraction peaks together with bright and clear electron diffraction spots (Figure 6D and inset).

3.2. Optical Waveguiding in Porphyrin Rectangular Microtube

One of the potential applications of enhanced PL from organic crystals is the organic optical waveguiding and amplified stimulated or spontaneous emission devices. The tetra(4-pyridyl)-porphyrin (H_2TPyP) rectangular microtube (RMT)

synthesized by *f*-PVT process is an example that exhibits not only enhanced PL but also amplified spontaneous emission (ASE).⁴² The H_2TPyP RMT crystal has well-developed crystalline facets that can be an effective light resonator cavity for ASE or lasing (Figure 7A). As shown in Figure 7B, the single H_2TPyP RMT shows bright PL emissions at both tips regardless of the position and type of photoexcitation (either epitaxial or focused spot illumination). Note that the emission intensity is measured using a confocal scanning microscope (CSM) coupled PL imaging system.

This result implies that the guided photon transport occurs along the tube growth axis and emits at the tip region. The ASE phenomenon from RMT is confirmed by monitoring abrupt increase of PL intensity upon the gradual increase of pumping laser power ($\lambda_{ex} = 410$ nm, Figure 7C). For example, the 0–1 band emissions from both tip and body are linearly increased up to 119 nJ of pump power. However, upon further increase of pump power to 200 nJ, the emission intensity from the tip is dramatically enhanced with narrowed full width at half-maximum (fwhm) of the peak while that from the body of RMT still shows linear increase (Figure 7C and D). The existence of pump threshold power at the tip is a promising

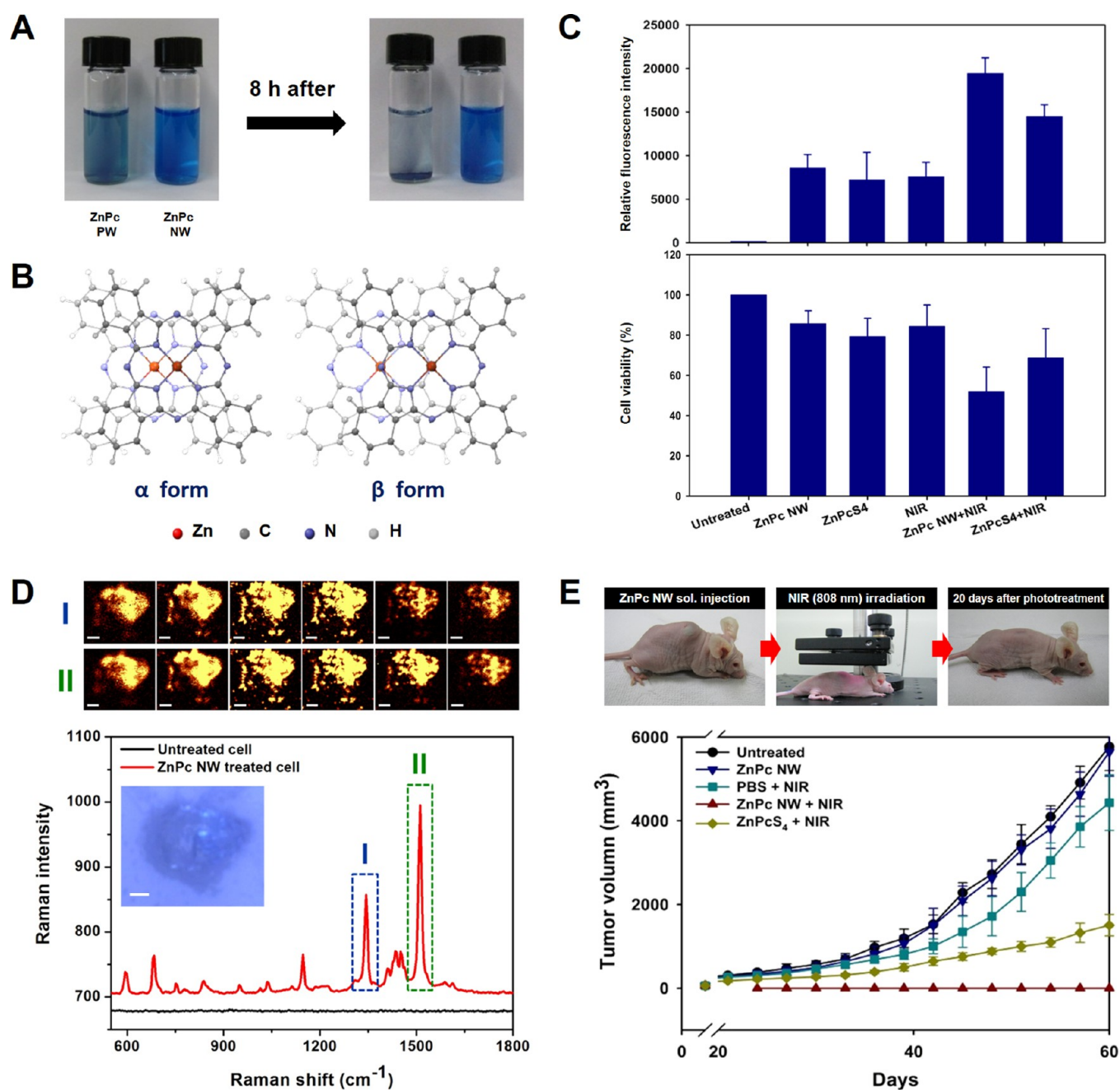


Figure 9. (A) Photograph showing stable dispersion of ZnPc NWs in water compared to ZnPc powder. (B) Superposition of ZnPc molecules in α -form and β -form. (C) In vitro cell experiments showing ROS generation (top) and cancer cell destruction (bottom) of water-dispersible ZnPc NW. (D) Confocal spectral images mapped with the peak intensities of two characteristic Raman features from ZnPc NW treated KB cancer cell (top) and corresponding Raman spectra. (E) In vivo photodynamic therapy and plot of average tumor volume changes as a function of observation time. Reproduced with permission from ref 8. Copyright 2012 Nature Publishing Group.

sign of new opportunities for the development of organic stimulated emission devices.

3.3. Morphology-Dependent Photoluminescence

Including the waveguiding and amplified spontaneous emission properties, most of the optical properties of organic crystals are highly dependent not only on the crystallinity but also on crystal morphology and molecular arrangement. Although the molecular arrangement-dependent emission property is an important research topic,^{43,44} the specific correlation between the optical property and crystal facet of a given geometry has been rarely reported. The prerequisite for this study is to

synthesize organic crystals having different morphologies with various crystal facets but still having same crystal structures. Pentacene 1D wire and 2D disks are good candidates for such purposes. Despite their identical crystal structure of triclinic ($P\bar{1}$),⁴⁵ only pentacene 1D wire shows strong PL emission from 560 to 760 nm while 2D disk has negligible PL (Figure 8A). Interestingly, careful investigation reveals that not all the pentacene 1D wires exhibit bright PL, but only the wires placed on a substrate with (010) crystal plane normal to the incident excitation light exhibit PL (Figure 8B, top and middle row). According to the SAED-PL correlated data (Figure 8B), the PL

inactive pentacene 1D wire turns out to have a (001) plane normal to the incident excitation light.¹¹

The PL activity depending on the crystal facet originates from the relative orientation of the dipole moment of pentacene molecules on a specific crystal plane to the direction of electric component of incident light. The dipole moment of pentacene on the (001) plane is almost perpendicular (72°) to the electric component of light, while it is almost parallel (18°) in the case of the (010) plane. The former case induces large absorption cross-section of incident light as confirmed by the absorption spectrum (Figure 8A, right), resulting in high PL intensity. On the other hand, the latter case forbids light absorption, leading to negligible PL (Figure 8A and C).

The presence of an optically active (010) plane in pentacene 1D wire promotes the electric photoresponse as well. As shown in Figure 8D, the photocurrent upon the irradiation of 365 nm light at a bias voltage of 10 V is remarkably increased from the device fabricated with a pentacene 1D wire having the (010) plane facing up.

3.4. Chemical Property Change: Water-Dispersible Zinc Phthalocyanine Nanowires (ZnPc NWs) for Cancer Phototherapy Application

The last case of the crystallization-induced property is the chemical property changes induced by the change of intermolecular interaction upon crystallization. The *f*-PVT process provides a great opportunity to explore new organic crystals having different intermolecular interactions, as the *f*-PVT process allows both thermodynamic and kinetic products of which crystal structures could be dissimilar to each other, leading to different intermolecular interaction power.

ZnPc, a potential candidate for the reactive oxygen species (ROS) generator upon near-infrared (NIR) light irradiation for photodynamic disease cell therapeutics, is intrinsically not soluble in water when it is present in powder form. In contrast, when ZnPc molecules are crystallized into ZnPc NWs by *f*-PVT process, they become highly dispersible in water with brief physical agitation. The ZnPc NW is stably dispersed in water for several months while most of ZnPc powder (PW) precipitates within a few hours as shown in Figure 9A. The unprecedented water dispersibility of ZnPc NW is quite remarkable considering that ZnPc NW is still composed of pure ZnPc molecules without any externally introduced hydrophilic moieties on the Pc backbones.

The key difference between ZnPc PW and ZnPc NW is their molecular packing patterns. According to the X-ray diffraction, high resolution TEM, and theoretical studies, ZnPc PW has a thermodynamically most stable β -form while ZnPc NW has an α -form crystal structure. As shown in Figure 9B, ZnPc molecules in α -form ZnPc NW are stacked as Zn(II) ions are slightly offset each other so that both hydrogen bonding and water coordination sites become available. In β -form ZnPc PW, however, all of the Zn(II) ions are coordinated to nitrogen atoms of adjacent ZnPc molecules, which prohibits additional coordination and hydrogen bonding to water molecules. The increased degree of water to ZnPc NW interaction via increased water coordination to Zn(II) ions and hydrogen bonding to nitrogen atoms in the Pc backbone are confirmed by UV-vis and FTIR studies.⁸

The water-dispersible ZnPc NW shows high photodynamic efficiency. The amount of ROS generated by ZnPc NW upon the irradiation of NIR ($\lambda = 808$ nm) is over 30% greater than other controls including commercially available ZnPcS₄ (Figure

9C, top). The dispersed ZnPc NW also shows high cell permeability as confocal micro-Raman imaging shows intense Raman signatures of ZnPc not only on the cancer KB cell surface but also inside the cell (Figure 9D). The in vitro cell experiment shows that more than 50% of cancer cell destruction occurs from the cells treated with ZnPc NW and NIR illumination. (Figure 9C, bottom). Finally, the phototherapeutic efficacy of ZnPc NW is evaluated through systematic in vivo experiments with tumor bearing mice. When ZnPc NW solution is locally injected into the tumor region at the tumor volume of 70 mm³ and irradiated with NIR laser (808 nm) for 3 min, the tumor growth is significantly suppressed, leading to complete eradication of the tumor while the tumor continuously grows in all other control groups (Figure 9E).

4. CONCLUSION

Highly conjugated molecular crystals in various morphologies offer opportunities to unveil their intrinsic optical and chemical properties that are differentiated according to specific crystal facets. This Account has focused on the synthesis of the morphologically well-defined crystals of highly conjugated organic and metal-containing organic molecules, and the crystallization-induced and morphology-dependent property changes from these crystals. The diversity of the crystal morphologies formed by *f*-PVT process is accomplished by overhauling thermodynamic barriers by designing growth systems allowing kinetic products. A similar success has been witnessed in solution phase reactions by carefully selecting solvent molecules and exploiting various phase interfaces, such as solid-liquid-air and liquid-liquid interfaces at which crystal growth occurs.

The studies on the optical, optoelectrical, and chemical properties of organic crystals show unprecedented features that have not been observed from their ensemble systems. The optical emission enhancement, waveguiding phenomenon, and drastic photocurrent increases originate from highly crystalline features with peculiar morphologies of the crystals. In addition, the increase in water-dispersibility of ZnPc NWs suggests a new tactic to resolve the low water solubility issue of photosensitizer for cancer therapeutic application. The property change emerging from morphology-controlled organic crystals is one of the core subjects toward the fundamental understanding of the intrinsic properties of organic crystals in various morphologies, and eventually for the development of high-performance organic molecule-based device applications.

■ AUTHOR INFORMATION

Corresponding Author

*E-mail: choihc@postech.edu.

Notes

The authors declare no competing financial interest.

Biographies

Chibeom Park received his B.S. in Material Science and Engineering at POSTECH in 2008 and his Ph.D. in Department of Chemistry at POSTECH. During his Ph.D course, he spent 1 year at Cornell University as a visiting student. He is currently a postdoctoral fellow at POSTECH studying the electrical properties of chemically doped carbon-based materials under the guidance of Prof. H. C. Choi.

Ji Eun Park received her B.S. in Chemistry from the Sookmyung Women's University in 2008 and her Ph.D. in 2014 at POSTECH

under the guidance of Prof. H. C. Choi. Her research interests are to synthesize conjugated organic crystals and to study the effects of geometry on their electrical/optical properties. She is currently a researcher at the Semiconductor R&D center of Samsung Electronics.

Hee Cheul Choi is a Hongdeok Young Chaired Professor in Department of Chemistry at POSTECH and Group Leader of Center for Artificial Low Dimensional Electronic Systems (CALDES) of Institute for Basic Science (IBS). Before he joined the faculty of Department of Chemistry at POSTECH in 2003, he obtained his Ph.D. in Chemistry from Purdue University (2001), then spent 2 years as a postdoctoral research associate at Stanford Chemistry. His work has encompassed many aspects of materials chemistry including synthesis, surface chemistry, device fabrications, and characterizations of carbon-based low dimensional and quantum scale structures. He received various awards including the Presidential Young Scientist Award (2009) and Distinguished Lectureship Award by the Chemical Society of Japan (2011).

ACKNOWLEDGMENTS

We acknowledge support from National Research Foundation (NRF) of Korea funded by Ministry of Science, ICT and Future Planning (2010-00285, 2013K2A2A40003581), and Ministry of Education (2009-0094036).

REFERENCES

- (1) Babu, S. S.; Möhwald, H.; Nakanishi, T. Recent progress in morphology control of supramolecular fullerene assemblies and its applications. *Chem. Soc. Rev.* **2010**, *39*, 4021–4035.
- (2) Shrestha, L. K.; Ji, Q.; Mori, T.; Miyazawa, K.; Yamauchi, Y.; Hill, J. P.; Ariga, K. Fullerene nanoarchitectonics: from zero to higher dimensions. *Chem.—Asian J.* **2013**, *8*, 1662–1679.
- (3) Shin, H. S.; Yoon, S. M.; Tang, Q.; Chon, B.; Joo, T.; Choi, H. C. Highly selective synthesis of C₆₀ disks on graphite substrate by a vapor-solid process. *Angew. Chem., Int. Ed.* **2008**, *47*, 693–696.
- (4) Park, C.; Song, H. J.; Choi, H. C. The critical effect of solvent geometry on the determination of fullerene (C₆₀) self-assembly into dot, wire and disk structures. *Chem. Commun.* **2009**, 4803–4805.
- (5) Kim, J.; Park, C.; Park, J. E.; Chu, K.; Choi, H. C. Vertical crystallization of C₆₀ nanowires by solvent vapor annealing process. *ACS Nano* **2013**, *7*, 9122–9128.
- (6) Park, C.; Yoon, E.; Kawano, M.; Joo, T.; Choi, H. C. Self-crystallization of C₇₀ cubes and remarkable enhancement of photoluminescence. *Angew. Chem., Int. Ed.* **2010**, *49*, 9670–9675.
- (7) Yoon, S. M.; Song, H. J.; Hwang, I.-C.; Kim, K. S.; Choi, H. C. Single crystal structure of copper hexadecafluorophthalocyanine (F₁₆CuPc) ribbon. *Chem. Commun.* **2010**, *46*, 231–233.
- (8) Moon, H. K.; Son, M.; Park, J. E.; Yoon, S. M.; Lee, S. H.; Choi, H. C. Significant increase in the water dispersibility of zinc phthalocyanine nanowires and applications in cancer phototherapy. *NPG Asia Mater.* **2012**, *4*, e12.
- (9) Tang, Q.; Li, H.; He, M.; Hu, W.; Liu, C.; Chen, K.; Wang, C.; Liu, Y.; Zhu, D. Low threshold voltage transistors based on individual single-crystalline submicrometer-sized ribbons of copper phthalocyanine. *Adv. Mater.* **2006**, *18*, 65–68.
- (10) Tong, W. Y.; Djurišić, A. B.; Xie, M. H.; Ng, A. C. M.; Cheung, K. Y.; Chan, W. K.; Leung, Y. H.; Lin, H. W.; Gwo, S. Metal phthalocyanine nanoribbons and nanowires. *J. Phys. Chem. B* **2006**, *110*, 17406–17413.
- (11) Park, J. E.; Son, M.; Hong, M.; Lee, G.; Choi, H. C. Crystal-plane-dependent photoluminescence of pentacene 1D wire and 2D disk crystals. *Angew. Chem., Int. Ed.* **2012**, *51*, 6383–6388.
- (12) Liu, H.; Li, Y.; Xiao, S.; Gan, H.; Jiu, T.; Li, H.; Jiang, L.; Zhu, D.; Yu, D.; Xiang, B.; Chen, Y. Synthesis of organic one-dimensional nanomaterials by solid-phase reaction. *J. Am. Chem. Soc.* **2003**, *125*, 10794–10795.
- (13) Wu, J. H.; Xu, T. Z.; Ang, S. G.; Xu, Q.-H.; Xu, G. Q. Radially oriented anthracene nanowire arrays: preparation, growth mechanism, and optical fluorescence. *Nanoscale* **2011**, *3*, 1855–1860.
- (14) Mei, J.; Diao, Y.; Appleton, A. L.; Fang, L.; Bao, Z. Integrated materials design of organic semiconductors for field-effect transistors. *J. Am. Chem. Soc.* **2013**, *135*, 6724–6746.
- (15) McQuarrie, D. A.; Simon, J. D. *Physical Chemistry: A Molecular Approach*; University Science Books: Sausalito, CA, 1997; pp 495–545.
- (16) Loi, M. A.; Como, E. D.; Dinelli, F.; Murgia, M.; Zamboni, R.; Biscarini, F.; Muccini, M. Supramolecular organization in ultra-thin films of α -sexithiophene on silicon dioxide. *Nat. Mater.* **2005**, *4*, 81–85.
- (17) Mattox, D. M. *Handbook of Physical Vapor Deposition (PVD) Processing*, 2nd ed.; Elsevier Science: Oxford, 2010; pp 195–235.
- (18) Briseno, A. L.; Mannsfeld, S. C. B.; Ling, M. M.; Liu, S.; Tseng, R. J.; Reese, C.; Roberts, M. E.; Yang, Y.; Wudl, F.; Bao, Z. Patterning organic single-crystal transistor arrays. *Nature* **2006**, *444*, 913–917.
- (19) Sree Harsha, K. S. *Principles of Physical Vapor Deposition of Thin Films*, 1st ed.; Elsevier Science: Oxford, 2005; pp 453–533.
- (20) Laudise, R. A.; Kloc, C.; Simpkins, P. G.; Siegrist, T. Physical vapor growth of organic semiconductors. *J. Cryst. Growth* **1998**, *187*, 449–454.
- (21) Kim, F. S.; Ren, G.; Jenekhe, S. A. One-dimensional nanostructures of π -conjugated molecular systems: assembly, properties, and applications from photovoltaics, sensors, and nanophotonics to nanoelectronics. *Chem. Mater.* **2011**, *23*, 682–732.
- (22) Reese, C.; Bao, Z. Organic single-crystal field-effect transistors. *Mater. Today* **2007**, *10*, 20–27.
- (23) Yoon, S. M.; Song, H. J.; Choi, H. C. p-Type semiconducting GeSe combs by a vaporization–condensation–recrystallization (VCR) process. *Adv. Mater.* **2010**, *22*, 2164–2167.
- (24) Yoon, S. M.; Hwang, I.-C.; Shin, N.; Ahn, D.; Lee, S. J.; Lee, J. Y.; Choi, H. C. Vaporization-condensation-recrystallization process-mediated synthesis of helical *m*-aminobenzoic acid nanobelts. *Langmuir* **2007**, *23*, 11875–11882.
- (25) Yoon, S. M.; Hwang, I.-C.; Kim, K. S.; Choi, H. C. Synthesis of single-crystal tetra(4-pyridyl)porphyrin rectangular nanotubes in the vapor phase. *Angew. Chem., Int. Ed.* **2009**, *48*, 2506–2509.
- (26) Lee, M.; Park, J. E.; Park, C.; Choi, H. C. Synthesis of a p-type semiconducting phenothiazine exfoliatable layered crystal. *Langmuir* **2013**, *29*, 9967–9971.
- (27) Kolb, H. C.; Sharpless, K. B. The growing impact of click chemistry on drug discovery. *Drug Discovery Today* **2003**, *8*, 1128–1137.
- (28) Northrup, J. E.; Tiago, M. L.; Louie, S. G. Surface energetics and growth of pentacene. *Phys. Rev. B* **2002**, *66*, 121404.
- (29) Haddon, R. C.; Hebard, A. F.; Rosseinsky, M. J.; Murphy, D. W.; Duclos, S. J.; Lyons, K. B.; Miller, B.; Rosamilia, J. M.; Fleming, R. M.; Kortan, A. R.; Glarum, S. H.; Makhija, A. V.; Muller, A. J.; Eick, R. H.; Zahurak, S. M.; Tycko, R.; Dabbagh, G.; Thiel, F. A. Conducting films of C₆₀ and C₇₀ by alkali-metal doping. *Nature* **1991**, *350*, 320–322.
- (30) Ganin, A. Y.; Takabayashi, Y.; Jeglič, P.; Arčon, D.; Potočnik, A.; Baker, P. J.; Ohishi, Y.; McDonald, M. T.; Tzirakis, M. D.; McLennan, A.; Darling, G. R.; Takata, M.; Rosseinsky, M. J.; Prassides, K. Polymorphism control of superconductivity and magnetism in Cs₃C₆₀ close to the Mott transition. *Nature* **2010**, *466*, 221–225.
- (31) Denning, M. S.; Watts, I. D.; Moussa, S. M.; Durand, P.; Rosseinsky, M. J.; Tanigaki, K. Close-packed C₇₀³⁻ phases – synthesis, structure, and electronic properties. *J. Am. Chem. Soc.* **2002**, *124*, 5570–5580.
- (32) Zhu, Q.; Cox, D. E.; Fischer, J. E.; Kniaz, K.; McGhie, A. R.; Zhou, O. Intercalation of solid C₆₀ with iodine. *Nature* **1992**, *355*, 712–714.
- (33) Pekker, S.; Kováts, É.; Oszlányi, G.; Bényei, G.; Klupp, G.; Bortel, G.; Jalsovszky, L.; Jakab, E.; Borondics, F.; Kamarás, K.; Bokor, M.; Kriza, G.; Tompa, K.; Faigel, G. Rotor-stator molecular crystals of fullerenes with cubane. *Nat. Mater.* **2005**, *4*, 764–767.

(34) Wang, L.; Liu, B.; Liu, D.; Yao, M.; Hou, Y.; Yu, S.; Cui, T.; Li, D.; Zou, G.; Iwasiewicz, A.; Sundqvist, B. Synthesis of thin, rectangular C₆₀ nanorods using *m*-xylene as a shape controller. *Adv. Mater.* **2006**, *18*, 1883–1888.

(35) Geng, J.; Zhou, W.; Skelton, P.; Yue, W.; Kinloch, I. A.; Windle, A. H.; Johnson, B. F. G. Crystal structure and growth mechanism of unusually long fullerene (C₆₀) nanowires. *J. Am. Chem. Soc.* **2008**, *130*, 2527–2534.

(36) Sathish, M.; Miyazawa, K. Size-tunable hexagonal fullerene (C₆₀) nanosheets at the liquid-liquid interface. *J. Am. Chem. Soc.* **2007**, *129*, 13816–13817.

(37) Wei, L.; Yao, J.; Fu, H. Solvent-assisted self-assembly of fullerene into single-crystal ultrathin microribbons as highly sensitive UV-visible photodetectors. *ACS Nano* **2013**, *7*, 7573–7582.

(38) Ramm, M.; Luger, P.; Zobel, D.; Duczak, W.; Boeyens, J. C. A. Static disorder in hexagonal crystal structures of C₆₀ at 100 K and 20 K. *Cryst. Res. Technol.* **1996**, *31*, 43–53.

(39) Céolin, R.; Agafonov, V.; André, D.; Dworkin, A.; Szwarc, H.; Dugué, J.; Keita, B.; Nadjo, L.; Fabre, C.; Rassat, A. Fullerene C₆₀, 2CCl₄ solvate. A solid-state study. *Chem. Phys. Lett.* **1993**, *208*, 259–262.

(40) Deegan, R. D.; Bakajin, O.; Dupont, T. F.; Huber, G.; Nagel, S. R.; Witten, T. A. Capillary flow as the cause of ring stains from dried liquid drops. *Nature* **1997**, *389*, 827–829.

(41) Miyazawa, K.; Kuwabara, M. C₆₀ nanowhiskers formed by the liquid–liquid interfacial precipitation method. *J. Mater. Res.* **2002**, *17*, 83–88.

(42) Yoon, S. M.; Lee, J.; Je, J. H.; Choi, H. C.; Yoon, M. Optical waveguiding and lasing action in porphyrin rectangular microtube with subwavelength wall thicknesses. *ACS Nano* **2011**, *5*, 2923–2929.

(43) Hinoue, T.; Shigenoi, Y.; Sugino, M.; Mizobe, Y.; Hisaki, I.; Miyata, M.; Tohnai, N. Regulation of π -stacked anthracene arrangement for fluorescence modulation of organic solid from monomer to excited oligomer emission. *Chem.—Eur. J.* **2012**, *18*, 4634–4643.

(44) Huang, L.; Liao, Q.; Shi, Q.; Fu, H.; Ma, J.; Yao, J. Rubrene micro-crystals from solution routes: their crystallography, morphology and optical properties. *J. Mater. Chem.* **2010**, *20*, 159–166.

(45) Mattheus, C. C.; Dros, A. B.; Baas, J.; Meetsma, A.; de Boer, J. L.; Palstra, T. T. M. Polymorphism in pentacene. *Acta Crystallogr.* **2001**, *C57*, 939–941.